ACS APPLIED MATERIALS & INTERFACES

Research Article

www.acsami.org

Facile Enhancement in CO-Tolerance of a Polymer-Coated Pt Electrocatalyst Supported on Carbon Black: Comparison between Vulcan and Ketjenblack

Zehui Yang,[†] ChaeRin Kim,[†] Shinsuke Hirata,[†] Tsuyohiko Fujigaya,[†] and Naotoshi Nakashima*[,†,‡,§]

[†]Department of Applied Chemistry, Graduate School of Engineering, Kyushu University, 744 Motooka, Nishi-ku, Fukuoka 819-0395, Japan

[‡]International Institute for Carbon Neutral Energy Research (WPI-I2CNER), Kyushu University, Fukuoka 819-0395, Japan

[§]Core Research for Evolutionary Science and Technology (CREST), Japan Science and Technology Agency (JST), 5 Sanbancho, Chiyoda-ku, Tokyo 102-0075, Japan

Supporting Information

ABSTRACT: The CO poisoning and low durability of the anode platinum electrocatalyst in the direct methanol fuel cell (DMFC) are the two crucial obstacles of the wide commercialization of the DMFC. In this study, we synthesized two different electrocatalysts using VulcanXC-72R (VC) and Ketjenblack (KB) as the carbon supporting material for the methanol oxidation reaction (MOR) and long-term durability test, in which the carbon supporting materials were wrapped by poly[2,2′-(2,6-pyridine)-5,5′-bibenzimidazole] (PyPBI) before the platinum deposition and the fabricated electrocatalysts were coated by the poly(vinylphosphonic acid) (PVPA) via the base-acid reaction. We have found that the as-prepared KB/PyPBI/Pt/PVPA shows a higher durability (7% loss in ECSA) under the potential cycling from 1.0 to 1.5 V vs. RHE compared to that of the VC/PyPBI/Pt/PVPA, which showed a 20% loss in ECSA after 10 000 cycle-durability test. Meanwhile, the KB/PyPBI/Pt/PVPA shows a higher CO tolerance before and after the durability test compared to that of the VC/PyPBI/Pt/PVPA, especially under very high methanol concentration (4 M and 8 M), which is close to the practical application of the DMFC. The observed higher CO tolerance is due to the higher amount of the PVPA (14.6 wt %) in the KB/PyPBI/Pt/PVPA caused by the higher specific surface area of the KB (1232 m^2/g) compared to the VC (235 m^2/g).

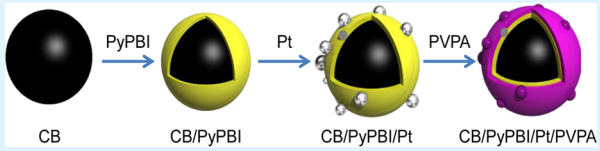

KEYWORDS: *Vulcan XC-72R, Ketjenblack, poly(vinylphosphonic acid), durability, CO tolerance*

INTRODUCTION

A growing demand for the efficient but low-cost sustainable energy has sparked significant interest in the commercial development of the fuel cell to replace the combustion-based energy.[1−3] Direct methanol fuel cells (DMFCs) have received considerable attention for the applications in the field of the electronic industries,[4,5] such as portable devices, because of the widely available fuel (methanol), high energy density (5500 Wh/kg),[6] and easy storage and transportation compared to hydrogen.[7] However, DMFC anode electrocatalysts still suffer from the following two main problems that hinder the widespread commercialization of DMFC, namely, (i) the carbon monoxide (CO) poisoning[8−11] caused by the incomplete oxidation of the methanol($Pt(CH_3OH)_{ads} \rightarrow Pt(CO)_{ads}+4H^+ +4e^-$)[10] and (ii) serious carbon corrosion ($C+2H_2O \rightarrow CO_2+4H^+ +4e^-$, 0.207 V vs. RHE),[12−14] which degrade the fuel cell performance during the operation.

Many researchers focused on the enhancement in the CO tolerance by using alloying platinum (Pt) with other transition metals, such as Ru,[15,16] Sn,[17,18] Mo,[19,20] Ni,[21,22] Co,[23,24] etc. However, such alloyed electrocatalysts have shown very low durability due to the dissolution of the transition metals in the real fuel cell operation.[25] Thus, the alloyed electrocatalysts are not suitable as a catalyst material in the real DMFC. Several groups have reported that CO tolerance of the electrocatalyst depended on the shape (semispherical, cubic, and tetrahedral-hexagonal) and facet of the Pt nanoparticles,[26−30] while these electrocatalysts suffered from a complex preparation method for the wide applications.

We have already reported a facile method to improve the CO tolerance and long-term durability simultaneously, in which the CB-based electrocatalyst was coated with an acidic polymer, poly(vinylphosphonic acid) (PVPA) that was assisted by a basic polymer poly[2,2′-(2,6-pyridine)-5,5′-bibenzimidazole] (PyPBI).[31] The PVPA weakened the binding energy between Pt-NP and CO species and accelerated the formation of the $Pt(OH)_{ads}$ due to the hydrophilic surfaces of the PVPA-coated electrocatalyst, which is considered to consume the $Pt(CO)_{ads}$ species on the electrocatalyst. Moreover, the methanol oxidation reaction (MOR) and long-term durability were further enhanced by decreasing the weight ratio between the Pt feeding and the polymer wrapped carbon support.[32]

Received: April 18, 2015
Accepted: July 6, 2015
Published: July 6, 2015

DOI: 10.1021/acsami.5b03371
ACS Appl. Mater. Interfaces 2015, 7, 15885−15891

However, the CO tolerance needs to be further enhanced and measured under high methanol concentration which is the real situation in the DMFC, because usually high methanol concentration is fed to the DMFC anode side to address the sluggish kinetic of the MOR.[33,34]

On the basis of the above considerations, here we synthesized two electrocatalysts, in which we used two different carbon supporting materials, Ketjenblack (KB) and Vulcan (VC), as schematically illuminated in Figure 1. The KB having

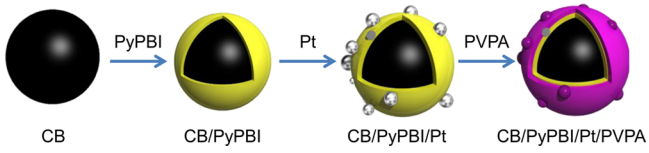

Figure 1. Schematic illustration for the preparation of the PVPA-coated electrocatalyst.

higher specific surface area is expected to use greater amount of the PyPBI to cover the surfaces and the greater amount of the PyPBI is expected to bind with large amount of the PVPA, which contributes to high CO tolerance. In this study, we compared the long-term durability and the CO tolerance evaluating in the MOR with different methanol concentration for the two electrocatalysts. The present study provides useful information about the preparation of a social demand state-of-the-art DMFC anodic electrocatalyst.

EXPERIMENTAL SECTION

Materials. Hydrogen hexachloroplatinatehexahydrate ($H_2PtCl_6 \cdot 6H_2O$), 2-propanol, *N,N*-dimethylacetamide (DMAc), ethylene glycol (EG), and poly(vinylphosphonic acid) (PVPA, 30 wt %) were purchased from Wako Pure Chemical Co., Ltd. Vulcan XC-72R and Ketjenblack (ECP600JD) were purchased from Cabot Chemical Co., Ltd. Pt-nanoparticle (NP)-deposited CB (CB/Pt) catalyst was purchased from Tanaka Kikinzoku Kogyo K. K., in which 37.9 wt % of Pt-NPs was supported on Vulcan XC-72R. Nafion solution (5 wt %) was purchased from Sigma-Aldrich. Perchloric acid ($HClO_4$, 70%) was obtained from EMD Millipore Chemical Co., Ltd. Methanol was purchased from Kanto Chemical Co., Inc. Poly[2,2′-(2,6-pyridine)-5,5′-bibenzimidazole] (PyPBI) was synthesized according to a previous report.[35] All aqueous solutions were made using Milli-Q water and all the chemicals were used as received without any further purification.

Synthesis of the CB/PyPBI/Pt. The KB/PyPBI (or VC/PyPBI) was synthesized according to our previous reports.[36−38] Briefly, the KB (or VC) was wrapped by PyPBI using sonication (Yamato 5510, Branson) for 1 h in DMAc. The composite was then collected by filtration, and then air-dried. Ten mg of the obtained KB/PyPBI (or VC/PyPBI) was dispersed in an EG aqueous solution (v/v = 3:2). Finally, the Pt loading was carried out by the reduction of the $H_2PtCl_6 \cdot 6H_2O$ (24 mg) in an EG aqueous solution (v/v = 3:2) at 140 °C for 6 h under a N_2 atmosphere. The obtained product was filtered, washed, and then dried overnight under vacuum at 60 °C to obtain the KB/PyPBI/Pt (or VC/PyPBI/Pt).

Synthesis of the CB/PyPBI/Pt/PVPA. Ten mg of the KB/PyPBI/Pt (or VC/PyPBI/Pt) was dispersed in a 10 mL EG aqueous solution (v/v = 3:2) by sonication for 5 min to which 1.0 mL of a 30 wt % PVPA aqueous solution was added, then ultrasonicated for 1h followed by filtration using a 0.1 μm PTFE filter paper to collect the solid product, which was washed several times with Milli-Q water to remove any physically bound PVPA, then dried overnight at 60 °C under vacuum to remove the residual solvent.

Characterization. The X-ray photoelectron spectroscopy (XPS) was carried out using an AXIS-ULTRA^{DLD} (Shimadzu) instrument. The pressure in the XPS analysis chamber was maintained at 1×10^{-9} Pa or lower during the measurement. In the calibration process, the binding energy (BE) of the core level C_{1s} peak was fixed at 284.5 eV. Elemental analysis was performed based on the regions of the C_{1s} (282−295 eV), N_{1s} (395−407 eV), Pt_{4f} (68−83 eV), and P_{2p} (127−139 eV) with the pass energy of 40 eV and linear background. The surface elemental compositions were determined by the ratios of peaks areas. Thermo gravimetric analysis (TGA) measurements were conducted using a TGA analyzer (EXSTAR 6000, Seiko Inc.) at the heating rate of 10 °C/min and 100 mL/min air-flow. TEM micrographs were measured using a JEM-2010 (JEOL, acceleration voltage of 120 kV) electron microscope. A copper grid with a carbon support (Okenshoji Co., Ltd.) was used for the TEM observations. Specific surface area was determined by the Brunauer−Emmett−Teller (BET) method based on N_2 adsorption isotherm measurements (77 K, $1 \times 10^{-8} < P/P_0 < 1$) using a BELSORP-mini (BEL Japan, Inc.) instrument. The gas adsorption measurements were conducted after pretreatment at 200 °C over 12 h under high vacuum.

Electrochemical Measurements. The electrochemical measurements were performed using a rotating ring disk electrode attached to an RRDE-3 (Bioanalytical Systems, Inc.) with a conventional three-electrode configuration in a vessel at room temperature. A glassy carbon electrode (GCE) with a geometric surface area of 0.196 cm^2 was used as the working electrode. A Pt wire and an Ag/AgCl were used as the counter and reference electrodes, respectively. The potential of the electrode was controlled by an ALS-Model DY2323 (BAS) potentiostat. The electrocatalyst suspension was typically prepared as follows. The catalysts (1.0 mg) were ultrasonically dispersed in each 80% 2-propanol aqueous solution (2.0 mL) to form homogeneous suspensions, which were cast on each GCE (the loading amount of Pt was controlled at 14 μg/cm^2), then air-dried. The cyclic voltammetry (CV) measurements of the electrocatalysts at the scan rate of 50 mV/s were carried in an N_2-saturated 0.1 M $HClO_4$ solution after 13 CV-cycles pretreatment with the scan rate of 5 mV/s in order to activate the electrocatalyst and to obtain a stable CV curve, and then the electrochemical surface area (ECSA) value was determined. All the potentials were referenced to the reference hydrogen electrode (RHE).

Durability Test. Carbon corrosion was tested using the protocol of the Fuel Cell Commercialization Conference of Japan (FCCJ)[39] (measured in N_2-saturated 0.1 M $HClO_4$ at room temperature without rotation), in which the potential was maintained at 1.0 V vs. RHE for 30 s, then applied 1.5 V vs. RHE a the scan speed of 0.5 V/s, followed by potential return to 1 V vs. RHE. This procedure was cycled, and after every 1000 cycles, ECSA measurements were carried out three times to calculate the average value (see the Supporting Information, Figure S1).

MOR Evaluation. The methanol oxidation reaction (MOR) was evaluated before and after the durability test using N_2-saturated methanol and 0.1 M $HClO_4$ at the scan rate of 50 mV/s at room temperature without rotation. The electrode was the same as used for the ECSA measurements. The Pt loading amounts were controlled at 14 μg/cm^2. Before the MOR measurements, 50 cycles were carried out to activate the electrocatalysts and to obtain a stable curve.

CO Stripping. CO stripping voltammetry was performed by feeding the work electrode with N_2 for 60 min and the activation of the electrocatalyst was carried out by 13-times CV cycles, and then purged with CO gas (10%) for 60 min with the flow rate of 100 mL/min, while holding the working electrode potential at 0.2 V vs. RHE. After the adsorption, the CO was removed from the electrolyte, then changed to N_2 bubbling for 50 min. The CO stripping voltammogram was recorded with the scan rate of 50 mV/s.

RESULTS AND DISCUSSION

Before the Pt deposition, the N_2 adsorption/desorption isotherms of the KB and VC before and after PyPBI wrapping were measured, and the results are shown in Figure 2a, b. The specific surface areas calculated from the Brunauer−Emmett−Teller (BET) method are shown in Figure 2c. The specific surface areas of the pristine KB and VC were determined to be

DOI: 10.1021/acsami.5b03371
ACS Appl. Mater. Interfaces 2015, 7, 15885−15891

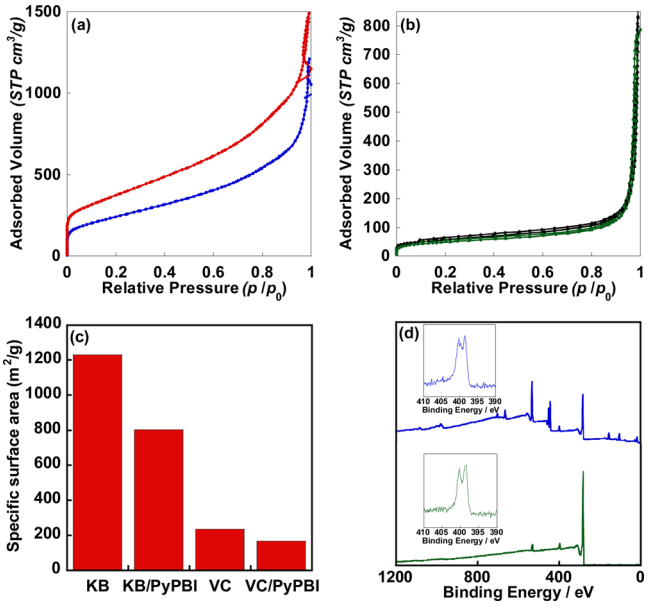

Figure 2. (a, b) N_2 adsorption/desorption isotherms of the KB (red line) and KB/PyPBI (blue line), VC (black line), and VC/PyPBI (green line). (c) Bar graphs demonstrate the specific surface areas of the KB and VC before and after PyPBI wrapping, which were calculated based on the BET method. (d) XPS spectra of the survey scan of the KB/PyPBI (blue line) and VC/PyPBI/Pt/PVPA (green line); the narrow scan of the region of the N_{1s} was displayed as the inset.

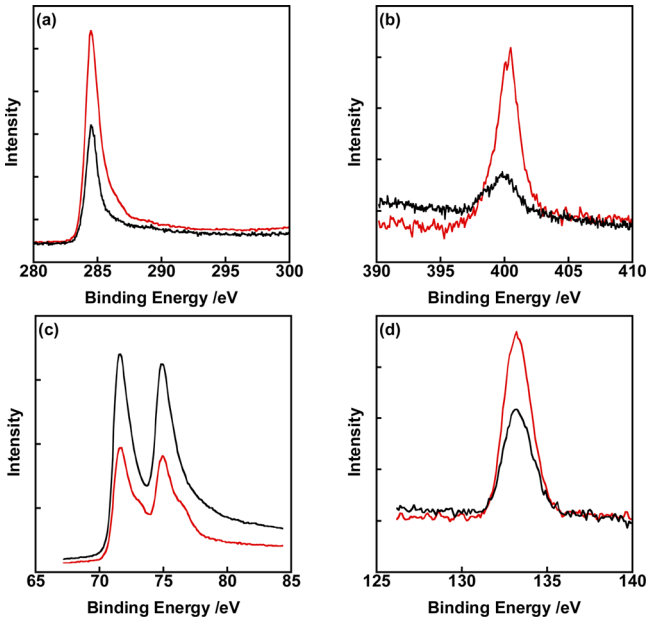

Figure 3. XPS narrow scans of regions of (a) C_{1s}, (b) N_{1s}, (c) Pt_{4f}, and (d) P_{2p} of the VC/PyPBI/Pt/PVPA (black line) and KB/PyPBI/Pt/PVPA (red line).

Table 1. Quantitative Analysis of the Surface Elemental Ratios of the VC/PyPBI/Pt/PVPA and KB/PyPBI/Pt/PVPA

sample	C (wt %)	Pt (wt %)	N (wt %)	P (wt %)
VC/PyPBI/Pt/PVPA	37.7	57.8	0.8	3.7
KB/PyPBI/Pt/PVPA	54.5	35.6	3.4	6.5

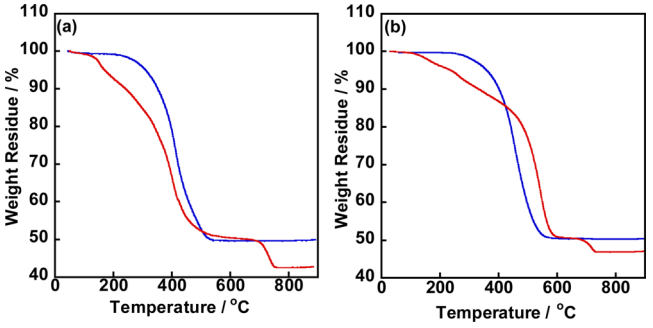

Figure 4. TGA curves of the (a) KB/PyPBI/Pt/PVPA and (b) VC/PyPBI/Pt/PVPA before (blue line) and after the PVPA coating (red line) measured under an air flow (100 mL/min) at a heating rate of 10 °C/min.

1232 and 235 m^2/g, respectively, which agreed with the previous report.[40] After wrapping with the PyPBI, the KB/PyPBI (805 m^2/g) still shows ~4.5 times higher specific surface area than that of the VC/PyPBI (176 m^2/g) as shown in Figure 2c. Also the two composites were monitored by the XPS to confirm the polymer wrapping. As shown in Figure 2d, we observed two N_{1s} peaks appeared at 398.0 and 399.0 eV that are attributed to be the pyridinic and pyrrolic nitrogen on the PyPBI, respectively, suggesting successful PyPBI-coating of the two carbon supports. The as-synthesized electrocatalysts were determined by the XPS measurements (for survey scan, see the Supporting Information, Figure S2). As shown in Figure 3a, sharp peaks are observed at 284.5 eV, which are assigned to the C_{1s} peaks of the carbon supports. As can be seen in Figure 3b, the typical N_{1s} peaks derived from PyPBI were appeared at 400 eV. Meanwhile, the Pt_{4f} peaks were detected at 71.1 and 74.4 eV shown in Figure 3c indicating that the main valence of the Pt species is zero.[41,42] As shown in Figure 3d, the typical P_{2p} peaks were observed at 133 eV, which is due to the PVPA. Interestingly, the intensities of the N_{1s} and P_{2p} peaks of the KB/PyPBI/Pt/PVPA were higher than those of the VC/PyPBI/Pt/PVPA, suggesting the presence of greater amounts of the PyPBI and PVPA in the KB/PyPBI/Pt/PVPA.[43,44] The quantitative analysis of the surface elemental ratios displayed in Table 1 indicated that the P and N in the KB/PyPBI/Pt/PVPA were 2 and 3.5 times higher than those in the VC/PyPBI/Pt/PVPA, respectively, which would be due to the larger specific surface area of the KB resulting in greater amount of the PyPBI to coat the surface of the carbon. Accordingly, greater amount of the PVPA was expected to coat on the PyPBI on the KB/PyPBI/Pt/PVPA via the acid−base reaction, which was confirmed by the TGA measurements, and the results are shown in Figure 4. The Pt contents in the KB/PyPBI/Pt and VC/PyPBI/Pt were comparable; namely, 49.5 and 50.4 wt % for the KB/PyPBI/Pt and VC/PyPBI/Pt, respectively, indicating Pt deposition on both carbon supports was very efficient. The PVPA amount was calculated from the decrease in the Pt content after coating with the PVPA because the ratio between KB/PyPBI (or VC/PyPBI) and Pt was almost the same before and after the PVPA coating. For the KB, the Pt content decreased from 49.5 wt % to 42.3 wt % due to 14.6 wt % of the additional PVPA, while, for the VC, the Pt content decreased from 50.4 wt % to 47.0 wt % and the PVPA amount was 6.7 wt %. The PVPA amount in the KB/PyPBI/Pt/PVPA was 2 times higher than that in the VC/PyPBI/Pt/PVPA, which agreed with the XPS quantitative analysis (see Table 1).

DOI: 10.1021/acsami.5b03371
ACS Appl. Mater. Interfaces 2015, 7, 15885−15891

On the basis of the Pt content, the electrochemical surface areas (ECSAs) were evaluated using eq 1

$$\text{ECSA} = Q_H/210(\text{Pt loading on the electrode}) \quad (1)$$

where Q_H is the charge exchanged during the electro-adsorption of the hydrogen on the Pt.[45−47]

The obtained ESCA values were 60.0 and 41.6 m^2/g for the KB/PyPBI/Pt/PVPA and VC/PyPBI/Pt/PVPA, respectively (see the Supporting Information, Figure S3a, b).The higher ECSA of the KB/PyPBI/Pt/PVPA was due to the smaller Pt-NPs size (2.8 ± 0.1 nm, Figure 5a) caused by the higher

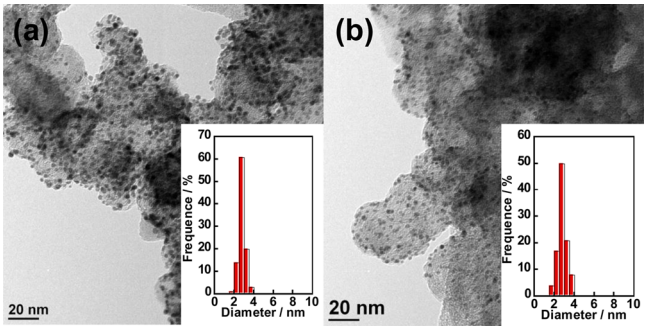

Figure 5. TEM images of the KB/PyPBI/Pt/PVPA (a) before and (b) after the durability test. Histograms of particle size distributions (100 particles) of the KB/PyPBI/Pt/PVPA before and after the durability test are shown as the inset.

specific surface area of the KB/PyPBI compared to the Pt deposited on the VC/PyPBI/Pt/PVPA (4.1 ± 0.3 nm, see the Supporting Information, Figure S4a), because all the PyPBI was considered to anchor the Pt-NP via the Pt−N bonding.[48,49]

The durability test of the electrocatalysts was simplified to evaluate the ECSAs in a 0.1 M $HClO_4$ solution after the potential cycling from 1.0 to 1.5 V vs. RHE to accelerate the oxidation of the carbon supporting material based on the protocol proposed by the Fuel Cell Commercialization Conference of Japan (FCCJ, see the Supporting Information, Figure S1). Interestingly, the KB/PyPBI/Pt/PVPA lost only by 7% of the initial ECSA after 10,000 cycles, while, the VC/PyPBI/Pt/PVPA showed 20%-loss in the ECSA, suggesting that the KB/PyPBI/Pt/PVPA has a higher durability compared to the VC/PyPBI/Pt/PVPA (see the Supporting Information, Figure S3c). Arenz et al. also reported that the Pt-NPs directly supported on KB were more durable than those on the VC because the VC exhibited a higher density of the surface defects, such as edges and corners of basal planes, where carbon corrosion was initiated due to the unsaturated valences and free electron density.[50] Interestingly, after the durability test, the Pt-NP size in the KB/PyPBI/Pt/PVPA was still 2.8 ± 0.2 nm as shown in Figure 5b, which was still smaller than that in the VC/PyPBI/Pt/PVPA (4.2 ± 0.5 nm, see the Supporting Information, Figure S4b).

High CO tolerance is very important for the anode electrocatalyst activity of the DMFC because the Pt-NPs on carbon supports are easily poisoned by CO species resulting in low performance. The CO tolerance is estimated from the I_f/I_b value (I_f and I_b are the anodic and reverse anodic peaks, respectively) of the CV curves of the electrocatalyst measured in a methanol solution.[51−53] The methanol oxidation reaction (MOR) was measured before and after durability test by continuously adding the methanol to the electrolyte. As shown in Figure 6a, b, the current densities of both I_f and I_b increased with the increase in methanol concentrations. The calculated I_f/I_b values were shown in the Table 2. The I_f/I_b ratios were found to decrease by 19% and 31% and with the increase in the methanol concentrations from 0.5 to 8 M before the durability test for the KB/PyPBI/Pt/PVPA and VC/PyPBI/Pt/PVPA, respectively, indicating that the methanol concentration

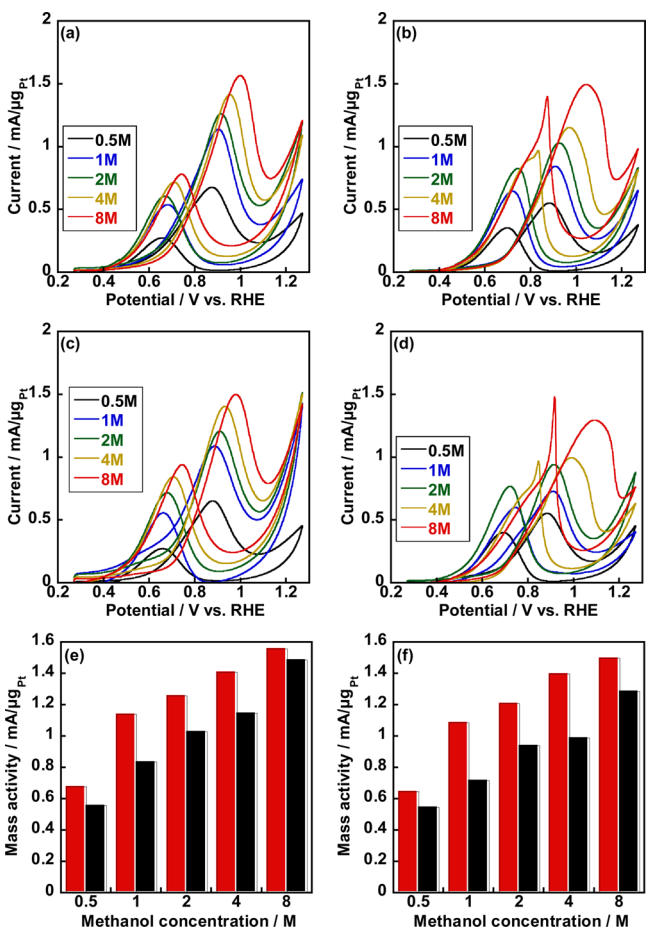

Figure 6. Methanol oxidation reaction (MOR) curves measured in an N_2-saturated 0.1 M $HClO_4$ and specified methanol concentration of the (a, c) KB/PyPBI/Pt/PVPA and (b, d) VC/PyPBI/Pt/PVPA before and after durability test. Mass activities of the KB/PyPBI/Pt/PVPA (red column) and VC/PyPBI/Pt/PVPA (black column) as a function of the methanol concentration (e) before and (f) after durability test.

Table 2. Comparisons of the KB/PyPBI/Pt/PVPA and VC/PyPBI/Pt/PVPA Regarding CO Tolerance (I_f/I_b Ratio) before and after Durability Test

electrocatalyst	0.5 M (I_f/I_b ratio)	1 M (I_f/I_b ratio)	2 M (I_f/I_b ratio)	4 M (I_f/I_b ratio)	8 M (I_f/I_b ratio)
KB/PyPBI/Pt/PVPA (before durability)	2.45	2.11	2.08	2.02	2.00
KB/PyPBI/Pt/PVPA (after durability)	2.39	1.96	1.69	1.67	1.63
VC/PyPBI/Pt/PVPA (before durability)	1.56	1.31	1.25	1.19	1.02
VC/PyPBI/Pt/PVPA (after durability)	1.38	1.21	1.2	1.03	0.87

DOI: 10.1021/acsami.5b03371
ACS Appl. Mater. Interfaces 2015, 7, 15885−15891

strongly affects the CO tolerance of the VC/PyPBI/Pt/PVPA compared to that of the KB/PyPBI/Pt/PVPA. Moreover, the KB/PyPBI/Pt/PVPA shows a high CO-tolerance in the specified methanol concentrations before the durability test. Under the high methanol concentration (8 M), which is close to the practical application of the DMFCs, the I_f/I_b ratio of the KB/PyPBI/Pt/PVPA was almost 2 and 3 times higher than those of the VC/PyPBI/Pt/PVPA and the commercial CB/Pt (see the Supporting Information, Figure S5 and Table S1), respectively. The higher CO tolerance would be due to the higher amount of the PVPA in the KB/PyPBI/Pt/PVPA, which facilitating the water adsorption on the Pt-NP surfaces to accelerate the formation of $Pt(OH)_{ads}$, which consumes the $Pt(CO)_{ads}$ and promoted the removal of the CO species from the catalyst. This was confirmed by the CO stripping voltammograms, in which the CO oxidation peak of the KB/PyPBI/Pt/PVPA shows a negative shift compared to that of the VC/PyPBI/Pt/PVPA as shown in Figure 7. After the durability

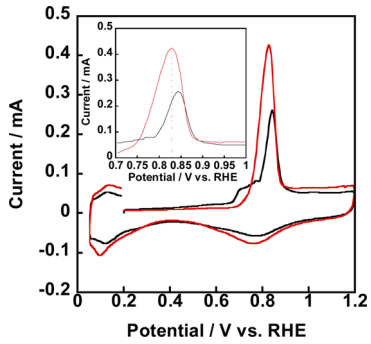

Figure 7. First cycle of the CO stripping voltammograms of the VC/PyPBI/Pt/PVPA (black line) and KB/PyPBI/Pt/PVPA (red line) at the scan rate of 50 mV/s at 25 °C. Zoom of the CO stripping profiles in 0.7−1.0 V vs. RHE are shown as the inset.

test, the I_f/I_b ratios decreased by 32% and 37% with the increase in the methanol concentration from 0.5 to 8 M for the KB/PyPBI/Pt/PVPA and VC/PyPBI/Pt/PVPA, respectively (see Table 2). Moreover, after the durability test, the I_f/I_b ratios of the KB/PyPBI/Pt/PVPA were also higher than those of the VC/PyPBI/Pt/PVPA, especially under high methanol concentrations (8 M), in which the value was still 2 times higher than that of the VC/PyPBI/Pt/PVPA. Such a high CO tolerance before and after durability test suggested that the electrocatalyst would be practically utilized in the DMFC anode side, in which high methanol concentration can be fed. The current densities of the I_f peak in MOR shown in Figure 6c, d decreased after the durability test due to the growth of the Pt-NP size. The mass current densities before and after the durability were shown in the Figure 6e, f. The mass current density of the KB/PyPBI/Pt/PVPA was higher than that of the VC/PyPBI/Pt/PVPA in the specified methanol concentration. Moreover, the KB/PyPBI/Pt/PVPA showed almost no loss in the mass activity, whereas the VC/PyPBI/Pt/PVPA lost by 10% of the initial mass activity. The onset potentials of the MOR in the different methanol concentrations of the KB/PyPBI/Pt/PVPA shows negative shifts compared to that of the VC/PyPBI/Pt/PVPA before and after the durability test (see the Supporting Information, Figure S5) because of the smaller Pt-NP size, which is more active.

CONCLUSIONS

In conclusion, we compared two fabricated PVPA-coated electrocatalysts using different carbon support materials, Vulcan XC-72R and Ketjenblack having surface areas of 235 and 1,232 m^2/g, respectively. The Ketjenblack-based electrocatalyst having larger surface area led to the high usage of the PVPA assisted by the PyPBI via the acid−base reaction to coat the surface of the carbon support. The KB/PyPBI/Pt/PVPA showed a higher CO tolerance compared to that of the VC/PyPBI/Pt/PVPA before and after the durability test, which would be due the higher amount of the PVPA (14.6 wt %), especially under a higher methanol concentration. Moreover, the KB/PyPBI/Pt/PVPA showed a higher durability compared to the VC/PyPBI/Pt/PVPA. The present study has demonstrated that the use of the KB in the PVPA-coated electrocatalyst enhances the CO tolerance and long-term durability, which is very important to prepare a state-of-the-art DMFC anode electrocatalyst for practical applications.

ASSOCIATED CONTENT

Supporting Information

TEM images of the VC/PyPBI/Pt/PVPA before and after durability. Methanol oxidation reaction (MOR) of the commercial CB/Pt. The Supporting Information is available free of charge on the ACS Publications website at DOI: 10.1021/acsami.5b03371.

AUTHOR INFORMATION

Corresponding Author

*E-mail: nakashima-tcm@mail.cstm.kyushu-u.ac.jp.

Author Contributions

The manuscript was written through contributions of all authors. All authors have given approval to the final version of the manuscript.

Notes

The authors declare no competing financial interest.

ACKNOWLEDGMENTS

This work was supported in part by the Nanotechnology Platform Project (Molecules and Materials Synthesis) of the Ministry of Education, Culture, Sports, Science and Technology (MEXT) Japan and by The Japan Science and Technology Agency (JST) through its Center of Innovation Science and Technology-based Radical Innovation and Entrepreneurship Program (COI Program). Z.H.Y. acknowledges China Scholarship Council (CSC) for their support.

REFERENCES

(1) Koenigsmann, C.; Wong, S. S. One-dimensional Noble Metal Electrocatalysts: A Promising Structural Paradigm for Direct Methanol Fuel Cells. *Energy Environ. Sci.* **2011**, *4*, 1161−1176.

(2) Giddey, S.; Badwal, S. P. S.; Kulkarni, A.; Munnings, C. A Comprehensive Review of Direct Carbon Fuel Cell Technology. *Prog. Energy Combust. Sci.* **2012**, *38*, 360−399.

(3) Kamarudin, S. K.; Achmad, F.; Daud, W. R. W. Overview on The Application of Direct Methanol Fuel Cell (DMFC) for Portable Electronic Devices. *Int. J. Hydrogen Energy* **2009**, *34*, 6902−6916.

(4) Hyeon, T.; Han, S.; Sung, Y.-E.; Park, K.-W.; Kim, Y.-W. High-Performance Direct Methanol Fuel Cell Electrodes Using Solid-Phase-Synthesized Carbon Nanocoils. *Angew. Chem., Int. Ed.* **2003**, *42*, 4352−4356.

DOI: 10.1021/acsami.5b03371
ACS Appl. Mater. Interfaces 2015, 7, 15885−15891

(5) Tomita, A.; Nakajima, J.; Hibino, T. Direct Oxidation of Methane to Methanol at Low Temperature and Pressure in an Electrochemical Fuel Cell. *Angew. Chem., Int. Ed.* **2008**, *47*, 1462−1464.
(6) Kundu, A.; Jang, J. H.; Gil, J. H.; Jung, C. R.; Lee, H. R.; Kim, S. H.; Ku, B.; Oh, Y. S. Micro-Fuel Cells—Current Development and Applications. *J. Power Sources* **2007**, *170*, 67−78.
(7) Kimiaie, N.; Wedlich, K.; Hehemann, M.; Lambertz, R.; Muller, M.; Korte, C.; Stolten, D. Results of a 20 000 h Lifetime Test of a 7 kW Direct Methanol Fuel Cell (DMFC) Hybrid System - Degradation of the DMFC Stack and the Energy Storage. *Energy Environ. Sci.* **2014**, *7*, 3013−3025.
(8) Knights, S. D.; Colbow, K. M.; St-Pierre, J.; Wilkinson, D. P. Aging Mechanisms and Lifetime of PEFC and DMFC. *J. Power Sources* **2004**, *127*, 127−134.
(9) Kim, H.; Shin, S.-J.; Park, Y.-g.; Song, J.; Kim, H.-t. Determination of DMFC Deterioration During Long-Term Operation. *J. Power Sources* **2006**, *160*, 440−445.
(10) Samant, P. V.; Rangel, C. M.; Romero, M. H.; Fernandes, J. B.; Figueiredo, J. L. Carbon Supports for Methanol Oxidation Catalyst. *J. Power Sources* **2005**, *151*, 79−84.
(11) Wang, A.-L.; Xu, H.; Feng, J.-X.; Ding, L.-X.; Tong, Y.-X.; Li, G.-R. Design of Pd/PANI/Pd Sandwich-Structured Nanotube Array Catalysts with Special Shape Effects and Synergistic Effects for Ethanol Electrooxidation. *J. Am. Chem. Soc.* **2013**, *135*, 10703−10709.
(12) Maass, S.; Finsterwalder, F.; Frank, G.; Hartmann, R.; Merten, C. Carbon Support Oxidation in PEM Fuel Cell Cathodes. *J. Power Sources* **2008**, *176*, 444−451.
(13) Huang, S.-Y.; Ganesan, P.; Park, S.; Popov, B. N. Development of a Titanium Dioxide-Supported Platinum Catalyst with Ultrahigh Stability for Polymer Electrolyte Membrane Fuel Cell Applications. *J. Am. Chem. Soc.* **2009**, *131*, 13898−13899.
(14) Huang, S.-Y.; Ganesan, P.; Popov, B. N. Titania Supported Platinum Catalyst with High Electrocatalytic Activity and Stability for Polymer Electrolyte Membrane Fuel Cell. *Appl. Catal., B* **2011**, *102*, 71−77.
(15) Li, L.; Xing, Y. Pt−Ru Nanoparticles Supported on Carbon Nanotubes as Methanol Fuel Cell Catalysts. *J. Phys. Chem. C* **2007**, *111*, 2803−2808.
(16) Tong; Kim, H. S.; Babu, P. K.; Waszczuk, P.; Wieckowski, A.; Oldfield, E. An NMR Investigation of CO Tolerance in a Pt/Ru Fuel Cell Catalyst. *J. Am. Chem. Soc.* **2002**, *124*, 468−473.
(17) Liu, Z.; Jackson, G. S.; Eichhorn, B. W. PtSn Intermetallic, Core−Shell, and Alloy Nanoparticles as CO-Tolerant Electrocatalysts for H2 Oxidation. *Angew. Chem., Int. Ed.* **2010**, *49*, 3173−3176.
(18) Sims, C. M.; Ponce, A. A.; Gaskell, K. J.; Eichhorn, B. W. CO Tolerance of Pt and PtSn Intermetallic Electrocatalysts on Synthetically Modified Reduced Graphene Oxide Supports. *Dalton Trans.* **2015**, *44*, 977−987.
(19) Mukerjee, S.; Urian, R. C. Bifunctionality in Pt Alloy Nanocluster Electrocatalysts for Enhanced Methanol Oxidation and CO Tolerance in PEM Fuel Cells: Electrochemical and In situ Synchrotron Spectroscopy. *Electrochim. Acta* **2002**, *47*, 3219−3231.
(20) Santiago, E. I.; Camara, G. A.; Ticianelli, E. A. CO Tolerance on PtMo/C Electrocatalysts Prepared by the Formic Acid Method. *Electrochim. Acta* **2003**, *48*, 3527−3534.
(21) Antolini, E.; Salgado, J. R. C.; Gonzalez, E. R. The Methanol Oxidation Reaction on Platinum Alloys with the First Row Transition Metals: The Case of Pt−Co and −Ni Alloy Electrocatalysts for DMFCs: A Short Review. *Appl. Catal., B* **2006**, *63*, 137−149.
(22) Hsieh, C.-T.; Lin, J.-Y. Fabrication of Bimetallic Pt−M (M=Fe, Co, and Ni) Nanoparticle/Carbon Nanotube Electrocatalysts for Direct Methanol Fuel Cells. *J. Power Sources* **2009**, *188*, 347−352.
(23) Wakisaka, M.; Mitsui, S.; Hirose, Y.; Kawashima, K.; Uchida, H.; Watanabe, M. Electronic Structures of Pt−Co and Pt−Ru Alloys for CO-Tolerant Anode Catalysts in Polymer Electrolyte Fuel Cells Studied by EC−XPS. *J. Phys. Chem. B* **2006**, *110*, 23489−23496.
(24) Liu, L.; Pippel, E.; Scholz, R.; Gösele, U. Nanoporous Pt−Co Alloy Nanowires: Fabrication, Characterization, and Electrocatalytic Properties. *Nano Lett.* **2009**, *9*, 4352−4358.
(25) Wang, S.; Cochell, T.; Manthiram, A. Boron-doped Carbon Nanotube-supported Pt Nanoparticles with Improved CO Tolerance for Methanol Electro-oxidation. *Phys. Chem. Chem. Phys.* **2012**, *14*, 13910−13913.
(26) Solla-Gullón, J.; Vidal-Iglesias, F. J.; Herrero, E.; Feliu, J. M.; Aldaz, A. CO Monolayer Oxidation on Semi-spherical and Preferentially Oriented (100) and (111) Platinum Nanoparticles. *Electrochem. Commun.* **2006**, *8*, 189−194.
(27) Solla-Gullón, J.; Vidal-Iglesias, F. J.; Lopez-Cudero, A.; Garnier, E.; Feliu, J. M.; Aldaz, A. Shape-dependent Electrocatalysis: Methanol and Formic Acid Electrooxidation on Preferentially Oriented Pt Nanoparticles. *Phys. Chem. Chem. Phys.* **2008**, *10*, 3689−3698.
(28) Yin, A.-X.; Min, X.-Q.; Zhang, Y.-W.; Yan, C.-H. Shape-Selective Synthesis and Facet-Dependent Enhanced Electrocatalytic Activity and Durability of Monodisperse Sub-10 nm Pt−Pd Tetrahedrons and Cubes. *J. Am. Chem. Soc.* **2011**, *133*, 3816−3819.
(29) Minch, R.; Es-Souni, M. A Versatile Approach to Processing of High Active Area Pillar Coral- and Sponge-like Pt-nanostructures. Application to Electrocatalysis. *J. Mater. Chem.* **2011**, *21*, 4182−4188.
(30) Wang, S.; Jiang, S. P.; Wang, X.; Guo, J. Enhanced Electrochemical Activity of Pt Nanowire Network Electrocatalysts for Methanol Oxidation Reaction of Fuel Cells. *Electrochim. Acta* **2011**, *56*, 1563−1569.
(31) Yang, Z.; Berber, M. R.; Nakashima, N. A Polymer-coated Carbon Black-based Fuel Cell Electrocatalyst with High CO-tolerance and Durability in Direct Methanol Oxidation. *J. Mater. Chem. A* **2014**, *2*, 18875−18880.
(32) Yang, Z.; Hafez, I. H.; Berber, M. R.; Nakashima, N. An Enhanced Anode Based on Polymer-Coated Carbon Black for Use as a Direct Methanol Fuel Cell Electrocatalyst. *ChemCatChem* **2015**, *7*, 808−813.
(33) Li, X.; Faghri, A. Review and Advances of Direct Methanol Fuel Cells (DMFCs) Part I: Design, Fabrication, and Testing with High Concentration Methanol Solutions. *J. Power Sources* **2013**, *226*, 223−240.
(34) Zhao, X.; Yin, M.; Ma, L.; Liang, L.; Liu, C.; Liao, J.; Lu, T.; Xing, W. Recent Advances in Catalysts for Direct Methanol Fuel Cells. *Energy Environ. Sci.* **2011**, *4*, 2736−2753.
(35) Xiao, L.; Zhang, H.; Jana, T.; Scanlon, E.; Chen, R.; Choe, E. W.; Ramanathan, L. S.; Yu, S.; Benicewicz, B. C. Synthesis and Characterization of Pyridine-Based Polybenzimidazoles for High Temperature Polymer Electrolyte Membrane Fuel Cell Applications. *Fuel Cells* **2005**, *5*, 287−295.
(36) Matsumoto, K.; Fujigaya, T.; Yanagi, H.; Nakashima, N. Very High Performance Alkali Anion-Exchange Membrane Fuel Cells. *Adv. Funct. Mater.* **2011**, *21*, 1089−1094.
(37) Berber, M. R.; Hafez, I. H.; Fujigaya, T.; Nakashima, N. Durability Analysis of Polymer-coated Pristine Carbon Nanotube-based Fuel Cell Electrocatalysts Under Non-humidified Conditions. *J. Mater. Chem. A* **2014**, *2*, 19053−19059.
(38) Hafez, I. H.; Berber, M. R.; Fujigaya, T.; Nakashima, N. Enhancement of Platinum Mass Activity on the Surface of Polymer-wrapped Carbon Nanotube-Based Fuel Cell Electrocatalysts. *Sci. Rep.* **2014**, *4*, 6295.
(39) Ohma, A.; Shinohara, K.; Iiyama, A.; Yoshida, T.; Daimaru, A. Membrane and Catalyst Performance Targets for Automotive Fuel Cells by FCCJ Membrane, Catalyst, MEA WG. *ECS Trans.* **2011**, *41*, 775−784.
(40) Sharma, S.; Pollet, B. G. Support Materials for PEMFC and DMFC Electrocatalysts—A Review. *J. Power Sources* **2012**, *208*, 96−119.
(41) Franceschini, E. A.; Planes, G. A.; Williams, F. J.; Soler-Illia, G. J. A. A.; Corti, H. R. Mesoporous Pt and Pt/Ru Alloy Electrocatalysts for Methanol Oxidation. *J. Power Sources* **2011**, *196*, 1723−1729.
(42) Franceschini, E. A.; Bruno, M. M.; Viva, F. A.; Williams, F. J.; Jobbágy, M.; Corti, H. R. Mesoporous Pt electrocatalyst for Methanol Tolerant Cathodes of DMFC. *Electrochim. Acta* **2012**, *71*, 173−180.
(43) Berber, M. R.; Fujigaya, T.; Nakashima, N. High-Temperature Polymer Electrolyte Fuel Cell Using Poly(vinylphosphonic acid) as an

DOI: 10.1021/acsami.5b03371
ACS Appl. Mater. Interfaces 2015, 7, 15885−15891

Electrolyte Shows a Remarkable Durability. *ChemCatChem* **2014**, *6*, 567−571.
(44) Berber, M. R.; Fujigaya, T.; Sasaki, K.; Nakashima, N. Remarkably Durable High Temperature Polymer Electrolyte Fuel Cell Based on Poly(vinylphosphonic acid)-doped Polybenzimidazole. *Sci. Rep.* **2013**, *3*, 1−7.
(45) Sun, S.; Zhang, G.; Geng, D.; Chen, Y.; Li, R.; Cai, M.; Sun, X. A Highly Durable Platinum Nanocatalyst for Proton Exchange Membrane Fuel Cells: Multiarmed Starlike Nanowire Single Crystal. *Angew. Chem., Int. Ed.* **2011**, *50*, 422−426.
(46) Wang, D.; Yu, Y.; Xin, H. L.; Hovden, R.; Ercius, P.; Mundy, J. A.; Chen, H.; Richard, J. H.; Muller, D. A.; DiSalvo, F. J.; Abruña, H. D. Tuning Oxygen Reduction Reaction Activity via Controllable Dealloying: A Model Study of Ordered Cu3Pt/C Intermetallic Nanocatalysts. *Nano Lett.* **2012**, *12*, 5230−5238.
(47) Wang, D.; Xin, H. L.; Hovden, R.; Wang, H.; Yu, Y.; Muller, D. A.; DiSalvo, F. J.; Abruña, H. D. Structurally Ordered Intermetallic Platinum−Cobalt Core−Shell Nanoparticles with Enhanced Activity and Stability as Oxygen Reduction Electrocatalysts. *Nat. Mater.* **2013**, *12*, 81−87.
(48) Okamoto, M.; Fujigaya, T.; Nakashima, N. Design of an Assembly of Poly(benzimidazole), Carbon Nanotubes, and Pt Nanoparticles for a Fuel-Cell Electrocatalyst with an Ideal Interfacial Nanostructure. *Small* **2009**, *5*, 735−740.
(49) Fujigaya, T.; Okamoto, M.; Nakashima, N. Design of an Assembly of Pyridine-containing Polybenzimidazole, Carbon Nanotubes and Pt Nanoparticles for a Fuel Cell Electrocatalyst with a High Electrochemically Active Surface Area. *Carbon* **2009**, *47*, 3227−3232.
(50) Speder, J.; Zana, A.; Spanos, I.; Kirkensgaard, J. J. K.; Mortensen, K.; Hanzlik, M.; Arenz, M. Comparative Degradation Study of Carbon Supported Proton Exchange Membrane Fuel Cell Electrocatalysts − The Influence of the Platinum to Carbon Ratio on the Degradation Rate. *J. Power Sources* **2014**, *261*, 14−22.
(51) Sun, X.; Li, D.; Ding, Y.; Zhu, W.; Guo, S.; Wang, Z. L.; Sun, S. Core/Shell Au/CuPt Nanoparticles and Their Dual Electrocatalysis for Both Reduction and Oxidation Reactions. *J. Am. Chem. Soc.* **2014**, *136*, 5745−5749.
(52) An, K.; Alayoglu, S.; Musselwhite, N.; Plamthottam, S.; Melaet, G.; Lindeman, A. E.; Somorjai, G. A. Enhanced CO Oxidation Rates at the Interface of Mesoporous Oxides and Pt Nanoparticles. *J. Am. Chem. Soc.* **2013**, *135*, 16689−16696.
(53) Guo, S.; Dong, S.; Wang, E. Three-Dimensional Pt-on-Pd Bimetallic Nanodendrites Supported on Graphene Nanosheet: Facile Synthesis and Used as an Advanced Nanoelectrocatalyst for Methanol Oxidation. *ACS Nano* **2010**, *4*, 547−555.

DOI: 10.1021/acsami.5b03371
ACS Appl. Mater. Interfaces 2015, 7, 15885−15891